

Probabilistic anatomical connectivity derived from the microscopic persistent angular structure of cerebral tissue

Geoffrey J. M. Parker^{1,*} and Daniel C. Alexander²

¹*Imaging Science and Biomedical Engineering, University of Manchester, Stopford Building, Oxford Road, Manchester M13 9PT, UK*

²*Department of Computer Science, University College London, Gower Street, London WC1E 6BT, UK*

Recently developed methods to extract the persistent angular structure (PAS) of axonal fibre bundles from diffusion-weighted magnetic resonance imaging (MRI) data are applied to drive probabilistic fibre tracking, designed to provide estimates of anatomical cerebral connectivity. The behaviour of the PAS function in the presence of realistic data noise is modelled for a range of single and multiple fibre configurations. This allows probability density functions (PDFs) to be generated that are parametrized according to the anisotropy of individual fibre populations. The PDFs are incorporated in a probabilistic fibre-tracking method to allow the estimation of whole-brain maps of anatomical connection probability. These methods are applied in two exemplar experiments in the corticospinal tract to show that it is possible to connect the entire primary motor cortex (M1) when tracing from the cerebral peduncles, and that the reverse experiment of tracking from M1 successfully identifies high probability connection via the pyramidal tracts. Using the extracted PAS in probabilistic fibre tracking allows higher specificity and sensitivity than previously reported fibre tracking using diffusion-weighted MRI in the corticospinal tract.

Keywords: anatomical connectivity; persistent angular structure; tractography; magnetic resonance imaging; diffusion-weighted imaging; probabilistic methods

1. INTRODUCTION

Probabilistic methods for determining the connectivity between brain regions using information obtained from diffusion-weighted MRI (DWI) have recently been introduced (Tuch *et al.* 2001; Koch *et al.* 2002; Lazar & Alexander 2002; Parker *et al.* 2002*a–c*, 2003; Behrens *et al.* 2003; Parker & Alexander 2003*a,b*). These approaches utilize probability density functions (PDFs), defined at each point within the brain to describe the local uncertainty in fibre orientation. Each PDF is intended to capture the information available in a DWI dataset concerning the distribution of likely underlying fibre structure. Given an accurate voxel-wise PDF it should be possible to obtain the probability of anatomical connection, defined at the voxel scale, between any two points within the brain. This may be achieved using Monte Carlo approaches based on, for example, streamlines (Behrens *et al.* 2002; Lazar & Alexander 2002; Parker *et al.* 2002*a–c*, 2003) or energy-minimization methods, such as those presented by Tuch *et al.* (2000).

To date, PDFs used in probabilistic connectivity methods have either been determined from the single diffusion tensor model (Behrens *et al.* 2002; Koch *et al.* 2002; Lazar & Alexander 2002; Parker *et al.* 2002*a–c*, 2003), multi-tensor models (Parker & Alexander

2003*a,b*), or by using q -space approximations acquired from spatially under-sampled brain data (Tuch *et al.* 2000). The single tensor model of diffusion assumes that diffusive water molecule displacements are Gaussian distributed, which is a poor approximation where fibres cross, diverge or have high curvature. This can lead to overly conservative PDFs that reflect the ambiguous fibre-orientation information available when using the tensor or, worse, inaccurate PDFs that assign unwarranted likelihood to spurious fibre orientations. Multi-tensor methods can identify more than one fibre population within a voxel, but again require the use of an explicit model of the multi-fibre population, and to date have not shown the capability to distinguish more than two fibre populations per voxel (Tuch *et al.* 2002; Parker & Alexander 2003*a,b*). Q -Space methods such as diffusion spectrum imaging (DSI) are an attractive option because they have the potential to identify an unlimited spectrum of fibre populations within a voxel (Tuch *et al.* 2000). However, the requirement for a very high number of diffusion-weighted image acquisitions makes whole-brain DSI impractical at the resolution required for diffusion-based connectivity mapping. At best, low-resolution imaging or imaging over a restricted volume are the only options, which lead to tracking errors and the potential for missed long-range cerebral connections, respectively. Newer q -space methods, such as ‘ q ball’ (Tuch *et al.* 2003) and persistent angular structure (PAS)–MRI (Jansons & Alexander 2003), overcome the excessive data acquisition requirements of DSI by resolving

* Author for correspondence (geoff.parker@manchester.ac.uk).

One contribution of 21 to a Theme Issue ‘Multimodal neuroimaging of brain connectivity’.

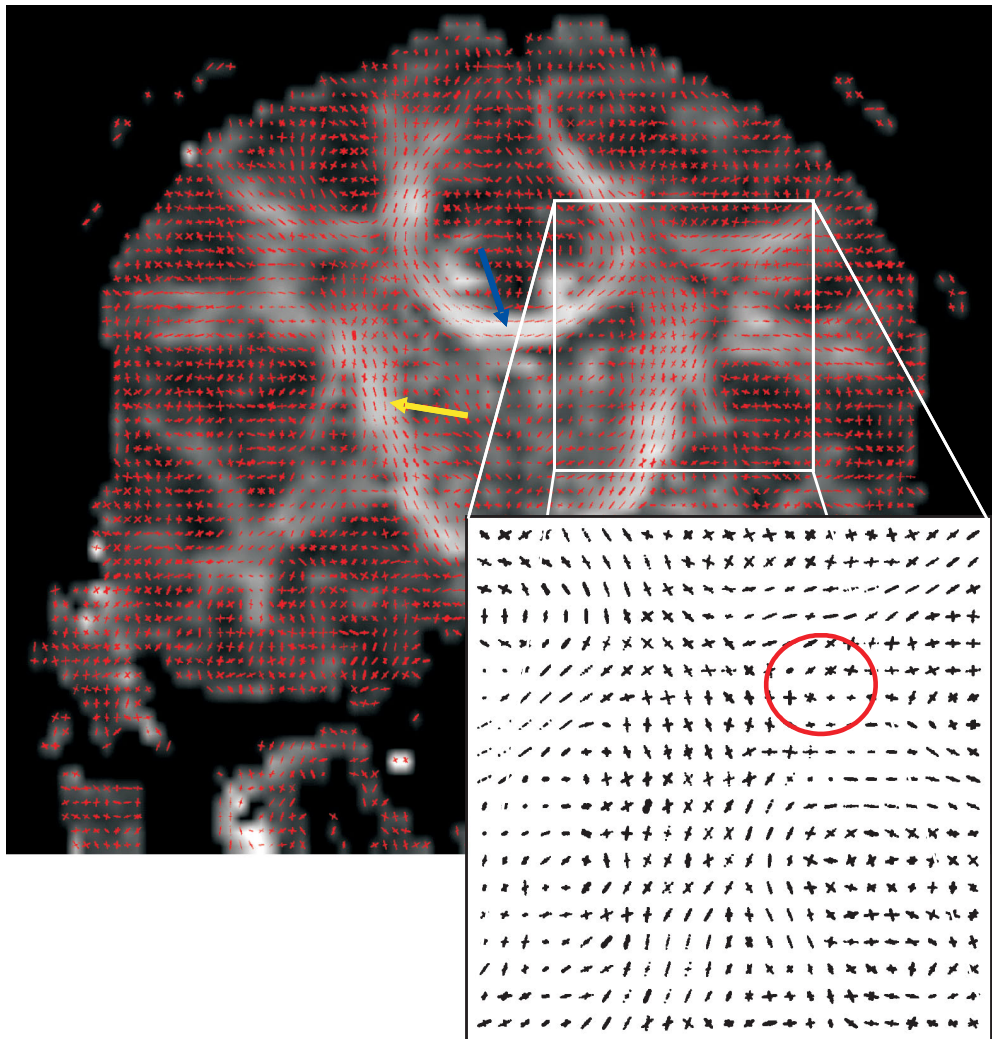


Figure 1. Fitted PAS functions in a coronal brain section overlaid on a fractional anisotropy (Pierpaoli & Basser 1996) map (note that the PAS function is tightly focused along identified orientations). The crossing fibres at the point where callosal fibres intersect corticospinal fibres (enlarged box) demonstrate mainly two-way crossings, but also a few three-way crossings (red circle). Also note the well-defined single fibre populations in, for example, the corpus callosum and corticospinal tract (blue and yellow arrows, respectively).

multiple fibre orientations within a voxel using data from the spherical acquisition schemes typical in diffusion tensor MRI (Jones *et al.* 1999). Such schemes allow routine whole-brain relatively high-resolution data acquisition, thus creating the possibility of extracting multiple fibre populations with manageable data acquisitions. Both q ball and PAS-MRI compute functions of the sphere that reflect the angular structure of the particle displacement density. The peaks of these functions provide estimates of fibre orientations. Neither of these methods has been used in probabilistic tracking to date. Here, we present a method for extracting probabilistic cerebral anatomical connectivity using the information provided by the PAS-MRI method for the first time, and demonstrate its utility in cerebral peduncle and precentral gyrus connectivity.

2. METHODS

(a) Data acquisition

Single-shot echo-planar diffusion-weighted brain data were acquired using a GE Signa 1.5 T scanner with a standard quadrature head coil. Sequence parameters were as follows: cardiac gating (repetition time = 20 cardiac cycles \sim 20 s), 60

Table 1. Eigenvalues used in the simulation of noise effects on estimated fibre orientation. (A constant value of trace = $2100 \times 10^{-6} \text{ mm}^2 \text{ s}^{-1}$ was used for all experiments.)

FA	$\lambda_1 (\times 10^{-6} \text{ mm}^2 \text{ s}^{-1})$	$\lambda_2, \lambda_3 (\times 10^{-6} \text{ mm}^2 \text{ s}^{-1})$
0.243	900	600
0.459	1100	500
0.635	1300	400
0.770	1500	300
0.870	1700	200
0.945	1900	100

axial slices, echo time = 95 ms, $N = 54$ unique gradient vectors \mathbf{g}_i , $i = 1, \dots, N$, each $|\mathbf{g}_i| = 22 \text{ mT m}^{-1}$ with gradient-pulse width $\delta = 34 \text{ ms}$ and pulse separation $\Delta = 40 \text{ ms}$, giving a b -factor for each of the N measurements of 1156 s mm^{-2} (calculated according to Stejskal & Tanner 1965) and $|\mathbf{q}| = \gamma \delta \mathbf{g} / 2\pi = 3.18 \times 10^4 \text{ m}^{-1}$, where γ is the gyromagnetic ratio. We also acquired six measurements with a b -factor $\sim 0 \text{ s mm}^{-2}$. We used a 96×96 acquisition matrix, interpolated during reconstruction to 128×128 ; 220 mm field of view, generating $2.30 \times 2.30 \times 2.30 \text{ mm}^3$ voxels as acquired, which were reconstructed to $1.72 \times 1.72 \times$

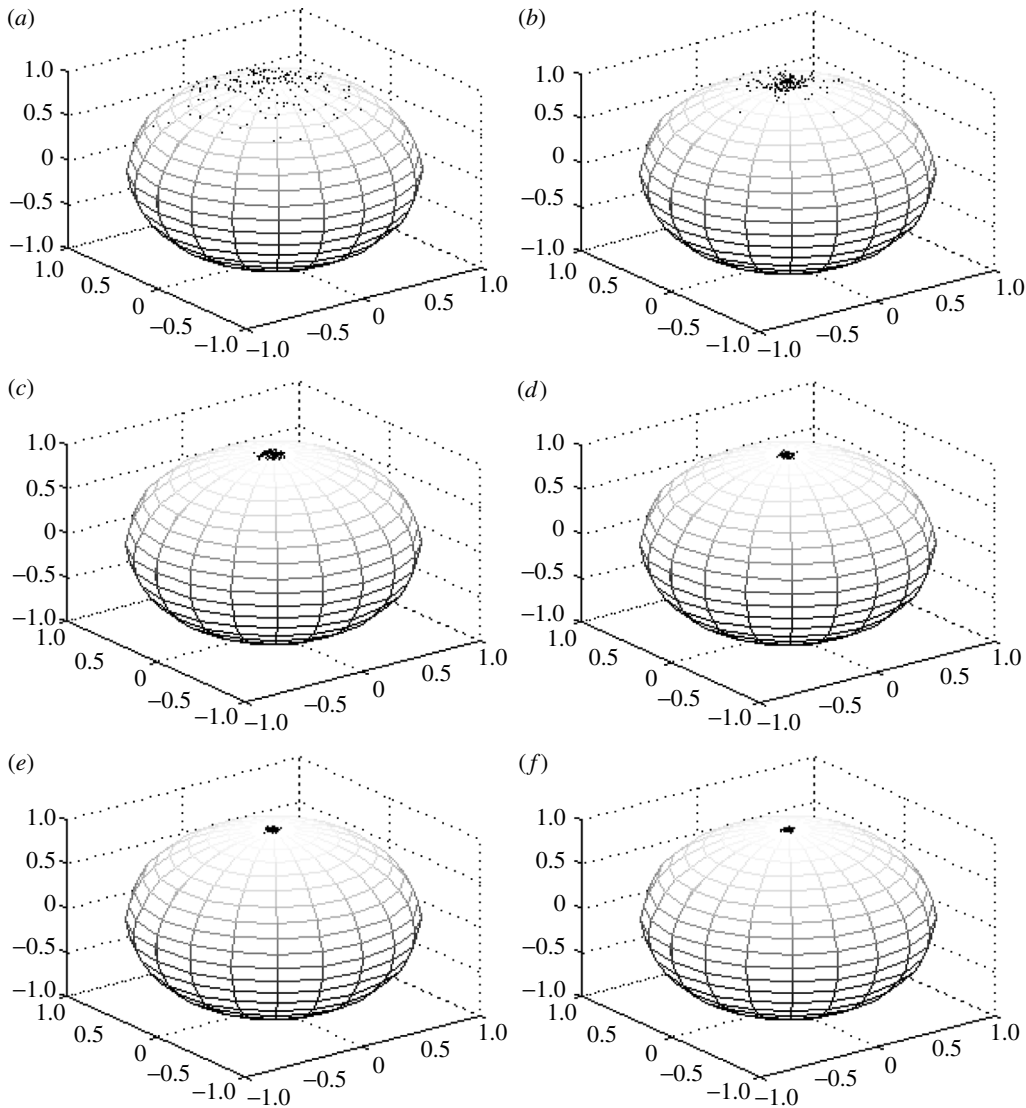


Figure 2. Simulated PAS-derived fibre-orientation distributions owing to random Gaussian-distributed noise plotted on the unit sphere for a range FA. Noiseless orientation of principal direction along vertical (z) axis. Cylindrical symmetry of all tensors is assumed. Simulation performed with a SNR of 16. (a) FA=0.243, (b) FA=0.459, (c) FA=0.635, (d) FA=0.770, (e) FA=0.870 and (f) FA=0.945.

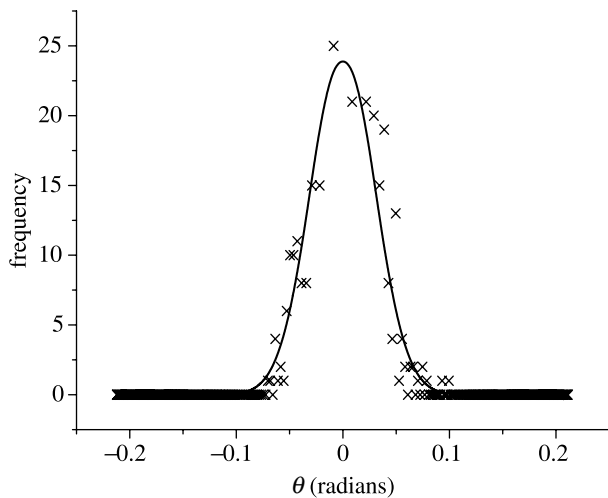


Figure 3. Distribution of deflection angle owing to noise added at SNR of 16 for single fibre case with FA=0.770 (see figure 2d).

2.30 mm³ (Wheeler-Kingshott *et al.* 2002). The acquisition time for the dataset was approximately 20 min. Eddy current induced image distortions in the diffusion-sensitized images were removed using affine multiscale two-dimensional registration (Symms *et al.* 1997).

All subjects were scanned with the approval of the joint National Hospital and Institute of Neurology ethics committee and gave informed, written consent. The signal-to-noise ratio (SNR) of the non-diffusion-weighted data in white matter in this data set is 16.

(b) Persistent angular structure

Features of a tissue’s microstructure may be inferred from the PDF p of diffusive water molecule displacements \mathbf{x} . In the absence of noise and when δ/Δ is negligible, the normalized diffusion-weighted measurement $S(\mathbf{q})/S(0)$ is the Fourier transform of p at wavenumber \mathbf{q} (Callaghan 1991). Assuming no net motion (flow) of spins, $p(\mathbf{x})=p(-\mathbf{x})$, so that:

$$\frac{S(\mathbf{q})}{S(0)} = \int_{\mathbb{R}^3} p(\mathbf{x})\cos(2\pi\mathbf{q}\cdot\mathbf{x})d\mathbf{x}. \tag{2.1}$$

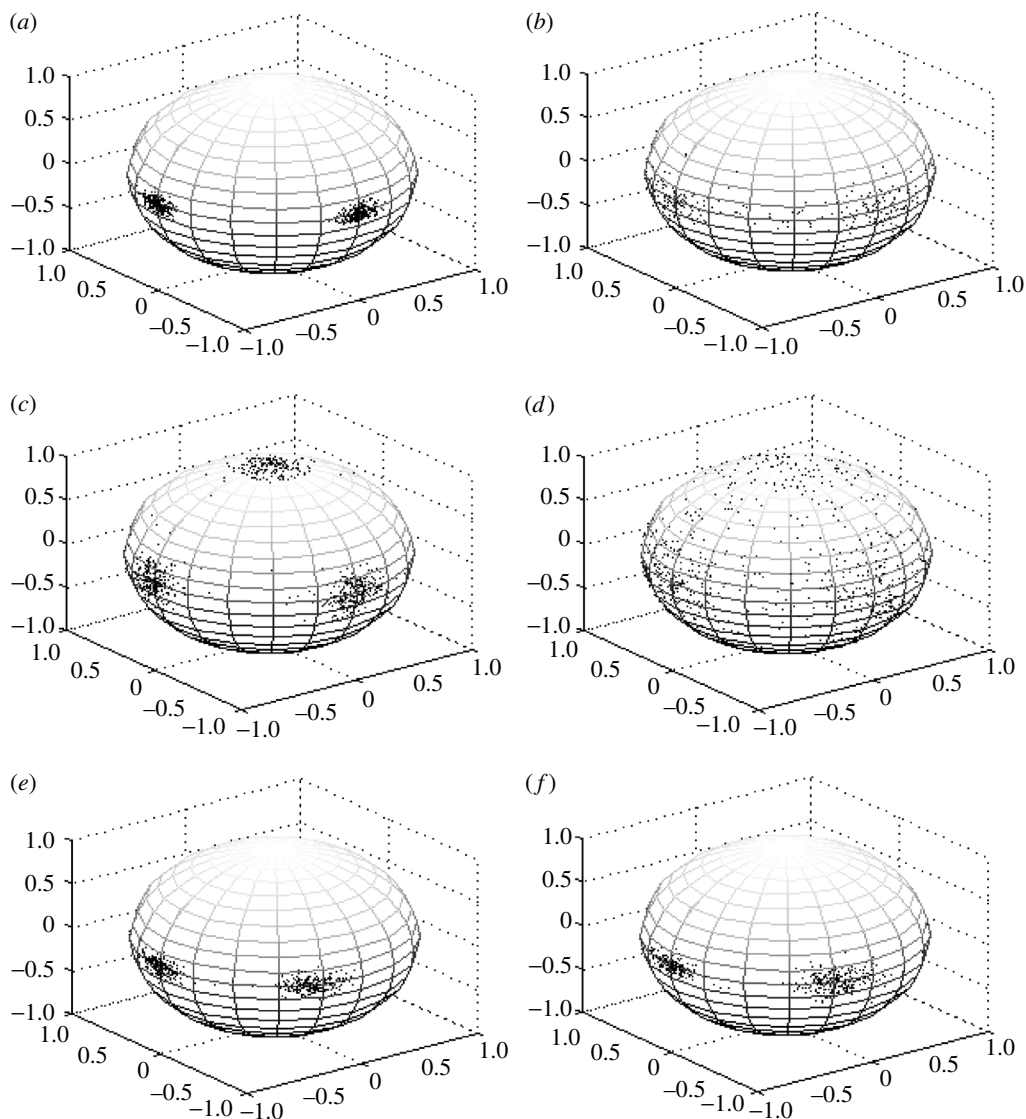


Figure 4. Simulated distributions of PAS-derived fibre orientations owing to random Gaussian-distributed noise plotted on the unit sphere for a range of crossing fibre cases. Cylindrical symmetry of all tensors is assumed and fibres are present in equal proportions. The simulation uses a SNR of 16. Noiseless fibre orientation: (a,b) x,y , (c,d) x,y,z , and (e,f) x , $\pi/8$ rotation from y . FA values for each tensor: (a,c,e) 0.770, (b,d) 0.459 and (f) 0.770 (along x), 0.635 (along $\pi/8$ rotation from y).

The PAS is the function on the sphere that, when embedded in three-space on a sphere of radius r , has the Fourier transform that best fits the measurements. We collapse the function p onto a sphere by using the approximation

$$p(\mathbf{x}) \approx \tilde{p}(\hat{\mathbf{x}})r^{-2}\delta(|\mathbf{x}| - r), \tag{2.2}$$

where δ is temporarily redefined as the standard one-dimensional δ distribution, $\hat{\mathbf{x}}$ is a unit vector in the direction of \mathbf{x} , and \tilde{p} is the PAS. Substituting equation (2.2) into equation (2.1) gives

$$\frac{S(\mathbf{q})}{S(\mathbf{0})} = \int \tilde{p}(\hat{\mathbf{x}})\cos(2\pi r\mathbf{q}\cdot\hat{\mathbf{x}})d\hat{\mathbf{x}}, \tag{2.3}$$

where the integral is now over the unit sphere.

Jansons & Alexander (2003) derive a maximum-entropy functional-form for the PAS

$$\tilde{p}(\hat{\mathbf{x}}) = \exp\left(\lambda_0 + \sum_{j=1}^N \lambda_j \exp(\mathbf{q}_j \cdot r\hat{\mathbf{x}})\right), \tag{2.4}$$

which is the product of $N + 1$ waves on the sphere; the \mathbf{q}_j , $j=1, \dots, N$, in equation (2.4) are the non-zero wavenumbers

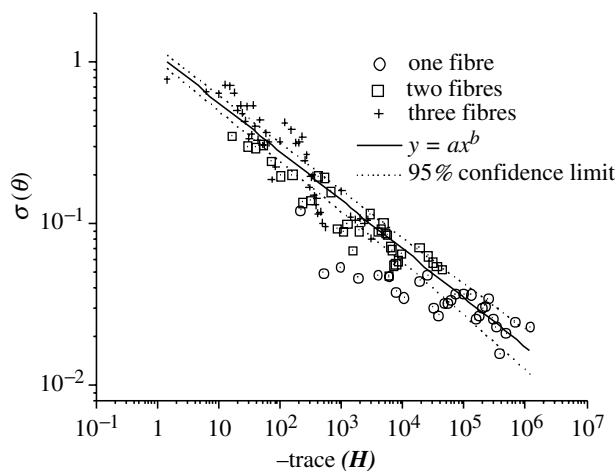


Figure 5. Standard deviation in θ owing to the addition of Gaussian noise at SNR of 16 as a function of $-\text{trace}(\mathbf{H})$.

sampled in the acquisition. A Levenberg–Marquardt algorithm finds the λ_i , $i=0, \dots, N$, that minimize the sum of squared errors between the N normalized measurements in a voxel and their estimates from equation (2.3). The integral in

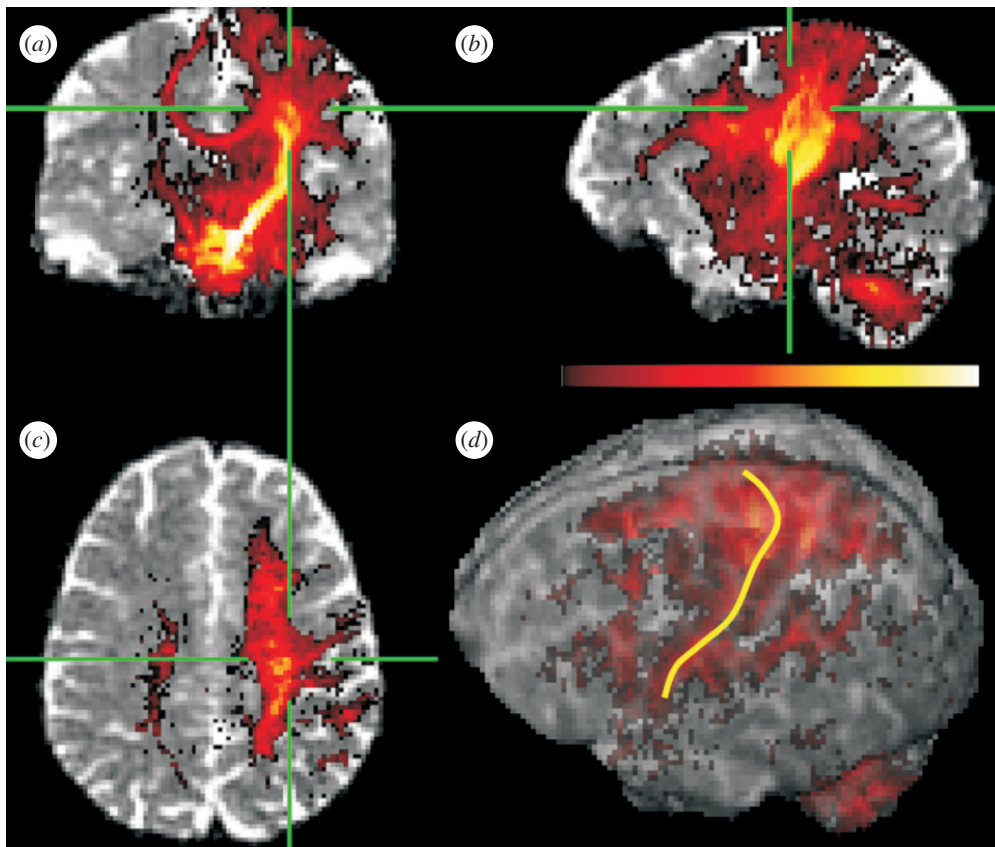


Figure 6. Maps of connection probability, Ψ , from a region of interest placed in the left cerebral peduncle, overlaid on $b=0$ echo planar image: (a) coronal, (b) sagittal, (c) axial views. Note branching of routes of connection to reach a range of cortical regions. (d) Cortical regions connected to left peduncle, overlaid on rendering of brain surface, viewed from left. Primary motor strip highlighted by yellow line. Radiological viewing convention used. Logarithmic colour scale: $0.02 < \Psi < 1.0$.

equation (2.3) is evaluated numerically for each \mathbf{q}_j . In general, for PAS-MRI the \mathbf{q}_j can be any set of wavenumbers, but here, since we use a spherical acquisition scheme, they all lie on a single shell in q -space.

The set of maxima of the PAS function that exceed a threshold provides the set of fibre-orientation estimates in a voxel. Figure 1 shows the PAS function in each voxel of a coronal section taken from a whole-brain data acquisition.

(c) Noise-based uncertainty in identified fibre orientations

The effect of noise on the PAS function in the case of single, two or three fibre populations is modelled using MR measurements synthesized from test functions (defined in §2(d)) that model p in each case. To generate noisy measurements, we add random complex samples drawn from independent zero-mean Gaussian distributions of the real and imaginary parts, each with standard deviation $S(\mathbf{0})/16$, to the Fourier transform of the test function at each \mathbf{q}_i sampled in the acquisition. We repeat this process to obtain a population of noisy signal intensity estimates, with which we estimate the PDFs for probabilistic tracking. We model the distribution of the angle of deflection θ of the estimated fibre direction with a zero-mean normal distribution. In the two and three fibre cases, we assume that the estimates for each fibre are independent and identically distributed.

(d) Fibre model

The test functions we use in the simulations are mixtures of Gaussian densities, which model the displacement density expected in the presence of single, two and three fibre

populations (Alexander *et al.* 2001; Frank 2002). Thus

$$p(\mathbf{x}) = \sum_{i=1}^n a_i ((4\pi\Delta)^3 \det(\mathbf{D}_i))^{-1} \exp[-\mathbf{x}^T \mathbf{D}_i^{-1} \mathbf{x} / 4\Delta], \quad (2.5)$$

where \mathbf{D}_i is the i th tensor, $n \leq 3$ and a_i are the relative proportions of each component ($\sum_{i=1}^n a_i = 1$). The degree of deflection of the fibre orientations identified using the PAS algorithm about their expected direction is dependent upon the noise level and the relative and absolute magnitudes of the tensor eigenvalues used in the simulation. Within the simulation we constrain the range of tensor eigenvalues since the trace of the diffusion tensor varies little in brain tissue. We reduce the simulation set further by assuming that the diffusion tensors have cylindrical symmetry around the principal axis, i.e. the three sorted eigenvalues have the property $\lambda_1 \geq (\lambda_2 = \lambda_3)$. In voxels exhibiting partial volume effects (for example, in the presence of crossing fibres), tensors not exhibiting this symmetry may be expected; however, as we are explicitly detecting and modelling crossing fibre cases, we assume that all remaining single tensors are cylindrically symmetric. We also assume that cases with two or three non-cylindrically symmetric tensors do not occur. Table 1 shows the sets of eigenvalues used for the simulation together with the tensor fractional anisotropy (FA; Pierpaoli & Basser 1996).

(e) Single fibre case

For the single cylindrically symmetric tensor simulation, the addition of Gaussian noise generates distributions in PAS-derived fibre orientation such as those shown in figure 2.

If we align the z -axis along the original principal diffusion direction, the PDF we obtain is independent of the angle ϕ of rotation around z and θ is approximately normally distributed with mean zero ($\theta \in [-\pi/2, \pi/2]$, $\phi \in [-\pi/2, \pi/2]$; figure 3).

(f) *Two and three fibre cases*

For mixture-model test functions with $n > 1$, the PAS function should have n peaks, one in the direction of the principal eigenvector of each component tensor. Examples of the distribution of the deflection of these peaks recovered from noisy data are shown in figure 4. The uncertainty associated with the PAS-derived fibre orientations when crossing fibres are present is larger than that in the single fibre case (figure 2), as a result of the added structural information that must be recovered from the same limited set of diffusion-weighted images. However, the mean orientation of each fibre is not affected by the presence of neighbouring fibre(s) at large angular separation. Furthermore, the spread in orientation of each is affected little by the relative orientation or spread of the other(s). With these observations we assume that the distributions of PAS-estimated fibre orientations for each fibre may be treated independently. As in the single fibre case, we use a Gaussian model for the distribution of the angle of deflection.

(g) *Parametrization of the fibre-orientation PDF*

The PDFs that we use for fibre tracking are normal distributions in θ (figure 3). We use the trace of the Hessian (\mathbf{H}) of the PAS at the peak, providing a fibre-orientation estimate to predict the standard deviation (σ_θ) of the normal distribution for that fibre-orientation estimate. To calibrate the mapping from trace(\mathbf{H}) to σ_θ , we calculate \mathbf{H} at each PAS peak recovered from the noisy synthetic data. The values of trace(\mathbf{H}) are sorted and binned into groups of 32 pairs of trace(\mathbf{H}) and the corresponding value of θ . We then compute the mean value of trace(\mathbf{H}) and the s.d. of θ within each bin. Figure 5 shows the relationship between trace(\mathbf{H}) and σ_θ , which is close to linear on the log-log plot. While the range of trace(\mathbf{H}) and σ_θ varies according to the number of fibre directions, the plot for each configuration approximately falls on the same line.

(h) *Streamline propagation in the multi-fibre field*

A step in the streamline propagation process is defined:

$$\mathbf{X}(l+1) = \mathbf{X}(l) + \mathbf{w}(l)\delta t, \quad (2.6)$$

where $\mathbf{X}(l)$ is the position in \mathcal{R}^3 of the streamline at point l on its length, $\mathbf{w}(l)$ is the propagation direction at point l and δt is the step size. We set $\mathbf{w}(l) = \mathbf{y}_m$, where $\mathbf{y}_1, \dots, \mathbf{y}_K$ are the fibre-orientation estimates from the PAS function at $\mathbf{X}(l)$ (as defined on each iteration of the Monte Carlo process (below) using the PDF interpolation scheme suggested by Behrens *et al.* (2003)) and m is the index $j=1, \dots, K$, for which $|\mathbf{y}_j \cdot \mathbf{w}(l-1)|$ is largest. This formulation ensures that when fibre crossing is detected, the PAS-derived fibre orientation closest to that of the current streamline propagation direction is chosen for further propagation (Blyth *et al.* 2003; Parker & Alexander 2003a,b). As a choice is being made between discrete estimates of separate fibre bundle orientations derived from the PAS PDF, the use of the maximum $|\mathbf{y}_j \cdot \mathbf{w}(l-1)|$ does not impose a strong curvature constraint on streamline propagation (as is seen in some diffusion tensor tracking methods: Poupon *et al.* 2000; Tuch *et al.* 2001; Mangin *et al.* 2002; Parker *et al.* 2002a-c).

(i) *Monte Carlo methods and maps of connection probability*

We use the PICo probabilistic-fibre-tracking framework to generate maps of connection probability (Parker *et al.* 2002a-c, 2003; Parker & Alexander 2003a,b). The method utilizes a Monte Carlo streamline approach, sampling the PDFs at each voxel location encountered by a streamline on each iteration; typically 1000 iterations are taken for each voxel within a start region (Toosy *et al.* 2004). The number of occasions, $\mu(\mathbf{p}, N)$, over N repetitions, at which each voxel \mathbf{p} is crossed by a streamline is used to define a map of the probability ψ of connection to the start point, in a similar fashion to that used by Koch *et al.* (2002):

$$\psi(\mathbf{p}) = \lim_{N \rightarrow \infty} \psi(\mathbf{p}, N) \approx \frac{\mu(\mathbf{p}, N)}{N}. \quad (2.7)$$

Maps of ψ are generated for each voxel within a user-defined tracking start region. The maps from each voxel are then combined into a connection probability union map, which describes the maximum value of $\psi(\mathbf{p})$ over all start voxels.

3. RESULTS

Two complementary experiments are presented in a healthy human volunteer's brain to demonstrate the effectiveness of noise-based probabilistic tracking using PAS-MRI. In the first, the pattern of connection probability from a region of interest covering the cross-section of the left cerebral peduncle is defined. In the second, the pattern of connection probability from a region covering the extent of the left primary motor strip is presented.

Figure 6 shows the connection probability union map to the region of interest covering the cross-section of the right cerebral peduncle. Branching of the extracted pathway may be observed at various points, with branches of relatively high probability to the medial and lateral primary motor cortex reaching the full extent of the primary motor strip. Similar levels of connection probability are also seen to the premotor areas, other frontal lobe areas and the thalamus. Non-zero connection probability may also be observed via the corpus callosum and the *trans*-pontine (pontocerebellar) fibres to the contralateral hemisphere.

A map of the voxels within the peduncle tracking start region that contribute to the connection probability union map in the precentral gyrus was generated (not shown). This indicates that the central portion of the peduncle has the highest connection probability to this region.

The results of an experiment using a start region of interest defined as the extent of the left precentral gyrus are shown in figures 7 and 8 at a range of connection probability thresholds. Figure 7 shows coronal projections of the connection probability union map. The highest probability connections observed are via the corticospinal tract to the left pyramid, to the thalamus, to the subthalamic nucleus, to the putamen, possibly to the globus pallidus, to Wernicke's area (see also figure 8), to the fornix and via the corpus callosum to the contralateral medial motor cortex. A number of lower probability connections are present; among the most prominent are connections to the cerebellar peduncles. Figure 8 shows the same connection

probability union map in sagittal projection at the same probability thresholds as those used in figure 7. The highest probability connections visible are via the pyramidal tract, to the superior parietal regions (Brodmann area 7), to the fornix, to the putamen and to Wernicke's area. The lower probability connections to the cerebellum observed in figure 7 are again visible.

4. DISCUSSION

We have identified voxels within the brain that include more than one fibre orientation and, by modelling the effects of noise, we have obtained PDFs on estimates of fibre orientation for the single, dual and triple fibre population cases. These PDFs are characterized as independent normal distributions in the angle of deflection away from the initial estimate of fibre orientation. The standard deviation of these distributions is related to the trace of the Hessian of the PAS function via an empirically derived power relationship.

Using the crossing fibre information, and the subsequently derived noise-based fibre-orientation PDFs, we have shown that it is possible to generate probabilistic representations of diffusion-based voxel-scale connectivity from user-defined start regions. This mapping benefits from the increased information content provided by PAS-MRI in comparison with diffusion tensor imaging, allowing more accurate definition of the routes and termini of connections. We have previously shown how single- and multi-tensor representations of the diffusion profile can also be used to generate PDFs of fibre orientation in the presence of crossing fibres (Parker & Alexander 2003a,b; Parker *et al.* 2003; Cook *et al.* 2004). However, in our experience this approach did not allow reliable identification of points in the brain showing three-way fibre crossings. Recent work by Tuch *et al.* (2003) has shown that it is possible to identify three-way crossings using the model-free q ball method. However, the q ball approach has been shown to require more angular samples of the diffusion profile, higher b values and greater SNR than PAS-MRI for reliable definition of a given number of fibre populations in a voxel (Alexander *in press*). Indeed, with the SNR used in this work, it has been shown by simulation that the PAS method should allow close to 100% sensitivity to orthogonal fibre crossings. This important advantage of the PAS-MRI method means that it is possible to extract multiple fibre population orientations using data such as those typically acquired in a clinical setting. However, the q ball method has the distinct advantage of significantly shorter computation times than current PAS-MRI implementations (Alexander 2004). The probabilistic tractography method we present here is straightforward to adapt for use with q ball reconstruction (or any other multiple-fibre reconstruction) rather than PAS-MRI (Parker & Alexander 2005).

The PAS-MRI technique displays a high degree of robustness to data noise, leading to PDFs of fibre orientation that show little dispersion at the levels of diffusion anisotropy expected in white matter tracts (figures 2 and 4). However, the noise levels in the data mean that the reliability with which multiple fibre

populations may be resolved decreases at small angular separations (Jansons & Alexander 2003). Our simulations suggest that at angular separations of less than 45 degrees we are able to satisfactorily resolve less than half of the test functions (data not shown). However, even with this limitation, it is clear that we are able to successfully resolve fibres at larger angular separation (figure 4) and that many fibre crossings are successfully identified *in vivo* (figure 1).

In this work we have focused on probabilistic tracking after accounting for crossing fibres. We have not explicitly attempted to account for non-Gaussian diffusion that may occur in fibres demonstrating high curvature or at points where fibre populations diverge. However, in these settings $|\text{trace}(\mathbf{H})|$ of the PAS function peak(s) is likely to be low, indicating relatively high uncertainty in fibre orientation (figure 5) and leading to dispersion of the probability of connection in both the diverging fibres case and the high curvature case. This is desirable for diverging fibre populations but not ideal for high curvature fibres, where the symmetry of the diffusion process currently restricts our knowledge of the polarity of fibre orientation. Also, we have not examined the effect of fibre populations of unequal proportions on the PAS-derived PDFs of fibre orientation, although the PAS function itself has been shown to be robust to a range of possible proportions (Alexander *in press*). This, and the development of methods to deal appropriately with high curvature, will form part of future work.

We have presented two complimentary experiments to demonstrate the utility of probabilistic fibre tracking using PAS-MRI. We have shown that the connections that pass via the cerebral peduncle may be reconstructed, and that these reconstructions to a large degree match what is expected from known anatomy. In particular, it is encouraging that the entire primary motor area is identified along the length of the precentral gyrus and showing marked lateral branching, as required to connect the mouth, face, eye and finger cortical areas. Although faithful reconstruction of this, the largest fibre tract of the brain, seems a trivial requirement for diffusion imaging-based fibre tracking, it has been shown consistently until now that the lateral motor areas are 'invisible' to fibre tracking from the cerebral peduncles (Clark *et al.* 2003; Hagemann *et al.* 2003; Hendler *et al.* 2003; Parker *et al.* 2003; Watts *et al.* 2003; Barrick & Clark 2004; Kuo *et al.* 2004; Lazar *et al.* 2004). The ability of PAS-MRI to extract multiple fibre populations at points in the corona radiata where it crosses the corpus callosum and the superior longitudinal fasciculus (figure 1), and the use of probabilistic fibre tracking are the key elements of this work that allow us to connect these lateral areas.

Other areas that are connected with high probability from the cerebral peduncle are the premotor areas, a number of other frontal lobe regions, some parietal lobe regions and the cerebellar peduncles. While the connections to the premotor area, the cerebellum and the sensory parietal regions are to be expected, the connections apparent in figure 6d to the ventrolateral frontal lobe in the vicinity of Broca's area are, to the best of our knowledge, unexpected. The thalamic

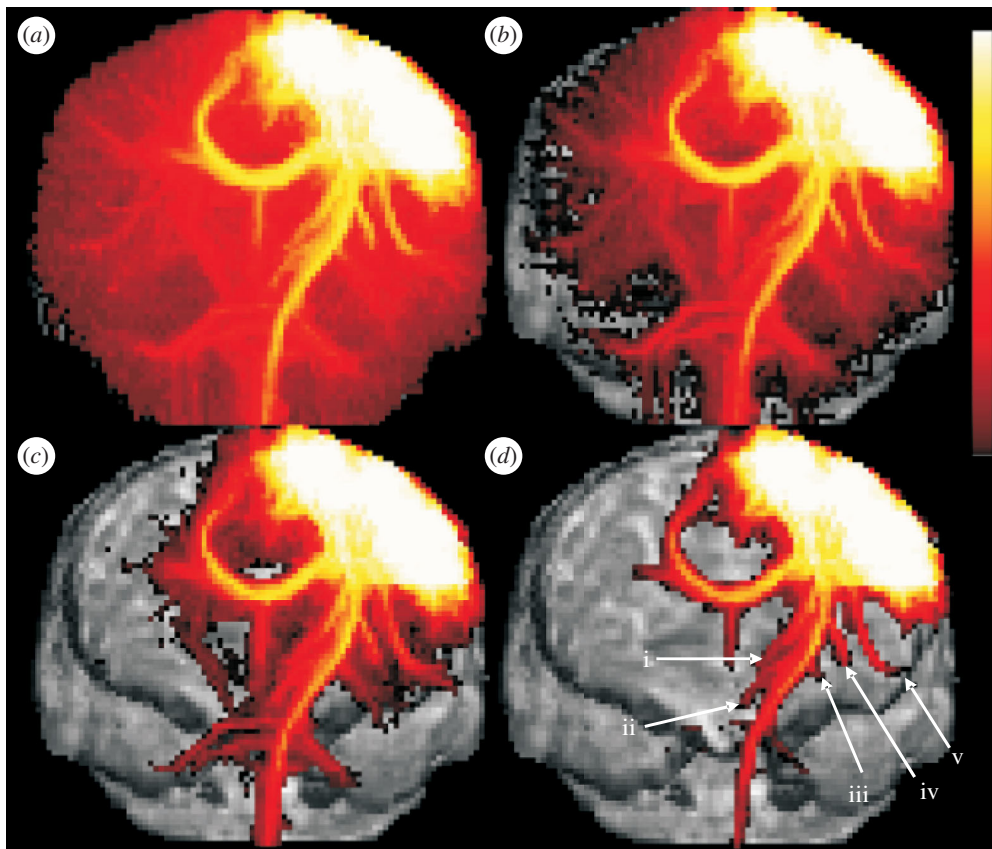


Figure 7. Coronal projections of left motor strip connectivity at different thresholds. Logarithmic colour scale: (a) $0.0 < \Psi < 1.0$, (b) $0.027 < \Psi < 1.0$, (c) $0.074 < \Psi < 1.0$ and (d) $0.20 < \Psi < 1.0$. Major apparent connections identified include: (i) thalamus, (ii) subthalamic nucleus, (iii) globus pallidus, (iv) putamen and (v) Wernicke's area (see figure 8).

connectivity observed from the cerebral peduncle in figure 6a is possibly due to partial volume of the corticospinal tracts with cerebellar pathways; it is possible that this is due to some overlap of the peduncle start region with the superior cerebellar peduncle, which could also contribute to the contralateral apparent connectivity. However, this could also arise from a partial volume effect with pathways entering the thalamus from the cerebral cortex.

The second experiment we present (figures 7 and 8) demonstrates two key points. First, that the probabilistic tracking process produces conjugate results—that is, that a tracking process from point A that reaches point B has a conjugate result that reaches point A from point B. This can be seen in the fact that the tracking from the cerebral peduncle connects to the entire primary motor area (figure 6d), and that the entire motor area, when used as a start region, connects via the peduncle (figures 7 and 8). A further experiment (results not shown), testing each motor cortex start-region component voxel separately for connection via the peduncle, indicated non-zero probability along the entire length of the motor cortex. The second key point is the high level of complexity of other identified connections from the motor cortex, including connections to the basal ganglia, parietal and frontal lobes. Thalamic connectivity from the motor strip appears, within the constraints of the resolution of the diffusion-weighted data, to be to the ventrolateral nucleus, the ventroposterolateral nucleus or the ventroposteromedial nucleus. Further connections are apparent to the

subthalamic nucleus (or possibly the substantia nigra) and the putamen. Each of these connections are, as expected, from known basal ganglia connectivity (Woolsey *et al.* 2003).

An unexpected finding in the tracking from the precentral gyrus is apparent connectivity to Wernicke's area, but a lack of connection to Broca's area, which is understood to have direct primary motor input. The Wernicke's connectivity may be owing to partial volume contamination as the corona radiata crosses the arcuate fasciculus in the centrum semiovale. The lack of connection to Broca's area presumably indicates a threshold in sensitivity for our method. Another unexpected connection is to the fornix, which may be seen clearly on figure 7. This appears to be due to partial volume mixing of this pathway with the corpus callosum at the midline.

Although the results we present are largely encouraging for the sensitivity and specificity of fibre tracking using DWI, there are still some limitations to the technique. It is clear from figures 6–8 that false positive and false negative connections are present in the results. The most significant of these are the contralateral pyramidal tract and corpus callosum involvement in the cerebral peduncle experiment (figure 6) and the Wernicke's area/middle temporal gyrus and fornix involvement in the precentral gyrus experiment (figures 7 and 8). None of these structures is likely to be connected anatomically to their respective start regions, yet the diffusion-weighted data, even using the PAS-MRI reconstruction, leads us to identify these

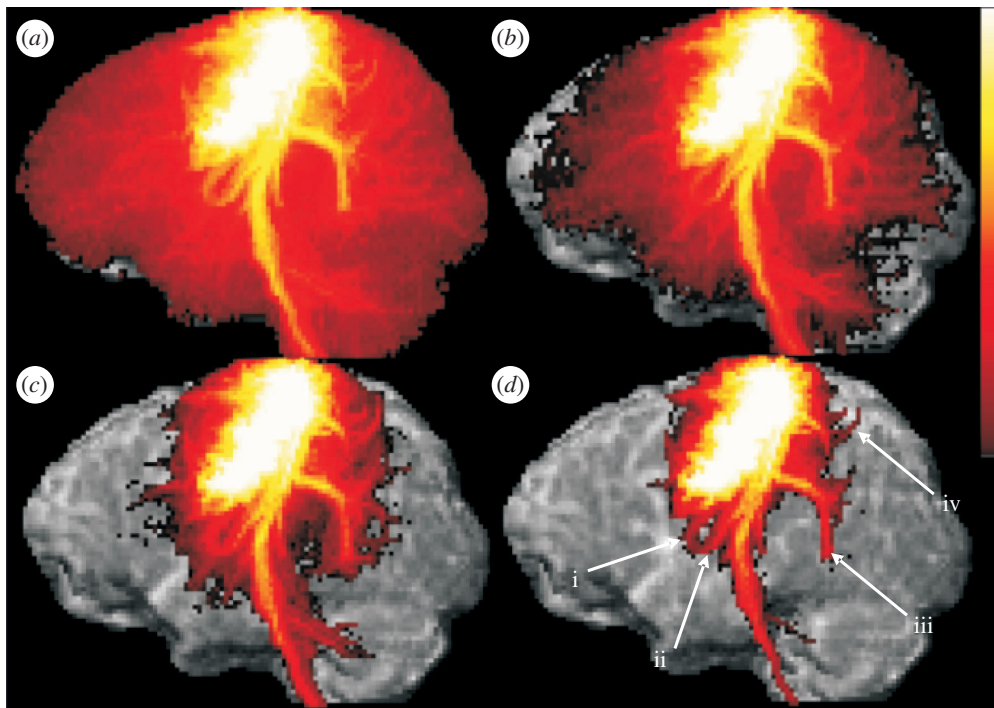


Figure 8. Sagittal projections of left motor strip connectivity at different thresholds. Logarithmic colour scale: (a) $0.0 < \Psi < 1.0$, (b) $0.027 < \Psi < 1.0$, (c) $0.074 < \Psi < 1.0$ and (d) $0.20 < \Psi < 1.0$. Major apparent connections identified include: (i) fornix, (ii) putamen (see figure 7), (iii) Wernike's area/middle temporal gyrus and (iv) superior parietal lobe.

as non-zero probability connections. It is likely that two major factors contribute to these errors. First, current understanding of the relationship between the observed diffusion-weighted signal, acquired at the voxel scale, and the characteristics of fibre bundle populations is incomplete. For example, although we are able to estimate the dominant diffusion orientations in an imaging voxel, we do not know with confidence how the observed diffusion profile is affected by axonal packing, the distribution of axonal diameters or the degree of myelination in a given fibre bundle. It is therefore currently impossible to estimate the density of connections between regions, and we may be more or less sensitive to some axonal configurations than others. Second, diffusion-weighted data acquisitions are at a relatively coarse spatial scale. Partial volume effects are unavoidable, and this leads to non-trivial problems in interpreting the diffusion-weighted signal. Although considerable improvements, including developments such as PAS-MRI, have been made in recent years in untangling the fibre orientation information present within a voxel, there are still certain fibre configurations that cannot currently be resolved satisfactorily. For example, if a number of fibre bundles converge to pass through a region of small cross-sectional area (as happens most obviously as the corticospinal tracts converge from the corona radiata to the pyramids) it becomes difficult to resolve the trajectories of the component bundles. When using probabilistic tracking methods, such situations tend to lead to dispersed patterns of low confidence connections downstream of the 'bottleneck' (see, for example, the cerebellar connections in the precentral gyrus experiment; figure 7). These limitations serve to remind us that the connection probability we define is one based on an interpretation of DWI data, rather

than an exact model of fibre tract structure. However, we are confident that future improved understanding of the relationship between fibre bundle structure and the diffusion-weighted signal, coupled with higher spatial resolution data acquisitions, will steadily increase the accuracy of probabilistic fibre-tracking results, allowing increasingly more sophisticated experiments to be carried out with this unique non-invasive method for mapping cerebral connections.

We are grateful to Dr Olga Ciccarelli and Dr Claudia Wheeler-Kingshott at the Institute of Neurology, London, for acquiring and making the data available.

REFERENCES

- Alexander, D. 2004 A comparison of q-ball and PASMRI on sparse diffusion MRI data. *Proc. Int. Soc. Magn. Res. Med.* 90.
- Alexander, D. C. In press. Multiple-fibre reconstruction algorithms for diffusion MRI. *Proc. N.Y. Acad. Sci.*
- Alexander, A. L., Hasan, K. M., Lazar, M., Tsuruda, J. S. & Parker, D. L. 2001 Analysis of partial volume effects in diffusion-tensor MRI. *Magn. Reson. Med.* **45**, 770–780.
- Barrick, T. R. & Clark, C. A. 2004 Singularities in diffusion tensor fields and their relevance in white matter fiber tractography. *NeuroImage* **22**, 481–491.
- Behrens, T. E. J., Jenkinson, M., Brady, J. M. & Smith, S. M. 2002 A probabilistic framework for estimating neural connectivity from diffusion weighted MRI. *Proc. Int. Soc. Magn. Reson. Med.* 1142.
- Behrens, T. E. J., Woolrich, M. W., Jenkinson, M., Johansen-Berg, H., Nunes, R. G., Clare, S., Matthews, P. M., Brady, J. M. & Smith, S. M. 2003 Characterization and propagation of uncertainty in diffusion-weighted MR imaging. *Magn. Reson. Med.* **50**, 1077–1088.
- Blyth, R., Cook, P. & Alexander, D. C. 2003 Tractography with multiple fibre directions. In *Proceedings of the Annual Meeting of the ISMRM*. Toronto: ISMRM, 240pp.

- Callaghan, P. T. 1991 *Principles of magnetic resonance microscopy*. Oxford: Oxford Science Publications.
- Clark, C. A., Barrick, T. R., Murphy, M. M. & Bell, B. A. 2003 White matter fiber tracking in patients with space-occupying lesions of the brain: a new technique for neurosurgical planning? *NeuroImage* **20**, 1601–1608.
- Cook, P., Parker, G. J. & Alexander, D. C. 2004 Modelling noise-induced fibre orientation error. *Proc. Int. Soc. Magn. Res. Med.* 1224.
- Frank, L. R. 2002 Characterization of anisotropy in high angular resolution diffusion-weighted MRI. *Magn. Reson. Med.* **47**, 1083–1099.
- Hagemann, P., Thiran, J.-P., Jonasson, L., Vandergheynst, P., Clarke, S., Maeder, P. & Meuli, R. 2003 DTI mapping of human brain connectivity: statistical fibre tracking and virtual dissection. *NeuroImage* **19**, 545–554.
- Hendler, T., Pianka, P., Sigal, M., Kafri, M., Ben-Bashat, D., Constantini, S., Graif, M., Fried, I. & Assaf, Y. 2003 “Two are better than one”: combining fMRI and DTI based fiber tracking for effective pre-surgical mapping. *Proc. Int. Soc. Magn. Reson. Med.* 394.
- Jansons, K. M. & Alexander, D. C. 2003 Persistent angular structure: new insights from diffusion magnetic resonance imaging data. *Inverse Probl.* **19**, 1031–1046.
- Jones, D. K., Horsfield, M. A. & Simmons, A. 1999 Optimal strategies for measuring diffusion in anisotropic systems by magnetic resonance imaging. *Magn. Reson. Med.* **42**, 515–525.
- Koch, M. A., Norris, D. G. & Hund-Georgiadis, M. 2002 An investigation of functional and anatomical connectivity using magnetic resonance imaging. *NeuroImage* **16**, 241–250.
- Kuo, L.-W., Wedeen, V. J., Weng, J.-C., Reese, T. G., Chen, J.-H. & Tseng, W.-T. I. 2004 Mapping white matter connectivity with BOLD activated regions using diffusion spectrum imaging and fMRI. *Proc. Int. Soc. Magn. Res. Med.* 1286.
- Lazar, M. & Alexander, A. L. 2002 White matter tractography using random vector (RAVE) perturbation. In *Proceedings of the Annual Meeting of the ISMRM*. Honolulu: ISMRM, 539pp.
- Lazar, M., Thottakara, P., Field, A. S., Laundre, B., Badie, B., Jellison, B. & Alexander, A. L. 2004 A white matter tractography study of white matter reorganization after surgical resection of brain neoplasms. *Proc. Int. Soc. Magn. Res. Med.* 1259.
- Mangin, J.-F., Poupon, C., Cointepas, Y., Papadopoulos-Orfanos, D., Clark, C. A., Regis, J. & Le Bihan, D. 2002 A framework based on spin glass models for the inference of anatomical connectivity from diffusion-weighted MR data—a technical review. *NMR Biomed.* **15**, 481–492.
- Parker, G. J. M. & Alexander, D. C. 2003a Probabilistic Monte Carlo based mapping of cerebral connections utilising crossing fibre information. *Proc. Int. Soc. Magn. Reson. Med.* 2932.
- Parker, G. J. M. & Alexander, D. C. 2003b Probabilistic Monte Carlo based mapping of cerebral connections utilising whole-brain crossing fibre information. *Lect. Notes Comput. Sci.* **2737**, 684–695.
- Parker, G. J. M. & Alexander, D. C. 2005 A mechanism for probabilistic fibre tracking using multi-fibre orientation functions. *ISMRM Workshop on Methods for Quantitative Diffusion MRI of the brain*. Lake Louise, Alberta, Canada, p. 74.
- Parker, G. J. M., Barker, G. J. & Buckley, D. L. 2002a A probabilistic index of connectivity (PICO) determined using a Monte Carlo approach to streamlines. *ISMRM Workshop on Diffusion MRI (Biophysical Issues)*, Saint-Malo, France, pp. 245–255.
- Parker, G. J. M., Barker, G. J., Thacker, N. A. & Jackson, A. 2002b A framework for a streamline-based probabilistic index of connectivity (PICO) using a structural interpretation of anisotropic diffusion. In *Proceedings of the Annual Meeting of the ISMRM*. Honolulu: ISMRM, 1165pp.
- Parker, G. J. M., Wheeler-Kingshott, C. A. M. & Barker, G. J. 2002c Estimating distributed anatomical brain connectivity using fast marching methods and diffusion tensor imaging. *IEEE Trans. Med. Imaging* **21**, 505–512.
- Parker, G. J. M., Haroon, H. A. & Wheeler-Kingshott, C. A. M. 2003 A framework for a streamline-based probabilistic index of connectivity (PICO) using a structural interpretation of MRI diffusion measurements. *J. Magn. Reson. Imaging* **18**, 242–254.
- Pierpaoli, C. & Basser, P. J. 1996 Toward a quantitative assessment of diffusion anisotropy. *Magn. Reson. Med.* **36**, 893–906.
- Poupon, C., Clark, C. A., Froulin, V., Regis, J., Le Bihan, D. & Mangin, J.-F. 2000 Regularization of diffusion-based direction maps for the tracking of brain white matter fascicles. *NeuroImage* **12**, 184–195.
- Stejskal, E. O. & Tanner, J. E. 1965 Spin diffusion measurements: spin echoes in the presence of a time-dependent field gradient. *J. Chem. Phys.* **42**, 288–292.
- Symms, M. R., Barker, G. J., Franconi, F. & Clark, C. A. 1997 Correction of eddy-current distortions in diffusion-weighted echo-planar images with a two-dimensional registration technique. In *Proceedings of the annual meeting of the ISMRM*. Vancouver: ISMRM, 1723pp.
- Toosy, A. T., Ciccarelli, O., Parker, G. J. M., Wheeler-Kingshott, C. A. M., Barker, G. J., Miller, D. H. & Thompson, A. J. 2004 Characterising function-structure relationships in the human visual system with functional MRI and diffusion tensor imaging. *NeuroImage* **21**, 1452–1463.
- Tuch, D. S., Belliveau, J. W. & Wedeen, V. J. 2000 A path integral approach to white matter tractography. In *Proceedings of the Annual Meeting of the ISMRM*. Denver: ISMRM, 791pp.
- Tuch, D. S., Wiegell, M. R., Reese, T. G., Belliveau, J. W. & Wedeen, V. J. 2001 Measuring cortico-cortical connectivity matrices with diffusion spectrum imaging. In *Proceedings of the Annual Meeting of the ISMRM*. Glasgow: ISMRM, 502pp.
- Tuch, D. S., Reese, T. G., Wiegell, M. R., Makris, N., Belliveau, J. W. & Wedeen, V. J. 2002 High angular resolution diffusion imaging reveals intravoxel white matter fiber heterogeneity. *Magn. Reson. Med.* **48**, 577–582.
- Tuch, D. S., Reese, T. G., Wiegell, M. R. & Wedeen, V. J. 2003 Diffusion MRI of complex neural architecture. *Neuron* **40**, 885–895.
- Watts, R., Holodny, A. I., Filippi, C. G. & Ulug, A. M. 2003 Sematotopic organization of motor fibers in the corticospinal tract—a combined fMRI and DTI Study. *Proc. Int. Soc. Magn. Reson. Med.* 395.
- Wheeler-Kingshott, C. A. M., Boulby, P. A., Symms, M. R. & Barker, G. J. 2002 Optimised cardiac gating for high angular-resolution whole-brain DTI on a standard scanner. *Proc. Int. Soc. Magn. Reson. Med.* 1118.
- Woolsey, T. A., Hanaway, J. & Gado, M. H. 2003 *The brain atlas*. Hoboken, NJ: Wiley.